The Egyptian Journal of Remote Sensing and Space Sciences 27 (2024) 524–531

Contents lists available at ScienceDirect

The Egyptian Journal of Remote Sensing and Space Sciences

journal homepage: www.sciencedirect.com

Research Paper

Geometric vs spectral content of Remotely Piloted Aircraft Systems images in the Precision agriculture context

Filippo Sarvia *, Samuele De Petris, Alessandro Farbo, Enrico Borgogno-Mondino

Department of Agricultural, Forest and Food Sciences, University of Turin, Grugliasco L.go Braccini 10095, Italy

ARTICLE INFO

Keywords:
Canopy height model
Precision farming
UAV
RPAS
Spectral index

ABSTRACT

In the last years the agricultural sector has been evolving and new technologies, like Unmanned Aerial Vehicles (UAV) and satellites, were introduced to increase crop management efficiency, reducing environmental costs and improving farmers' income. MAIA-S2 sensor is presently one of the most performing optical sensors operating on a Remotely Piloted Aircraft Systems (RPAS); given its spectral features, it aims at supporting a scaling process where monoscopic satellite data (namely Copernicus S2) with high temporal and limited geometric resolution can be integrated with stereoscopic data from RPAS having a very high spatial resolution. In this work, data from MAIA-S2 sensor were used to detect the effects of different fertilization types on corn with reference to a test field located in Carignano (Piemonte region, NW-Italy). Different amounts of top dressing fertilization were applied on corn and an RPAS acquisition operated on 14th June 2021 (corresponding date to the corn stem elongation stage) to explore if any effects could be detectable. Three spectral indices, namely Normalized Difference Vegetation Index, Normalized Difference Red Edge index and Canopy Height Model, computed from at-the-ground reflectance calibrated MAIA-S2 data, were compared to evaluate the correspondent response to the different fertilization rates. Results show that: (i) NDVI poorly detect N-related differences zones; (ii) NDRE and CHM reasonably reflect the different N fertilization doses; (iii) Only CHM proved to be able to detect crop height and, consequently, biomass differences that are known to be induced by different rates of fertilization.

1. Introduction

Precision agriculture (PA) has been defined as a new type of agriculture that looks for climate, environmental, economic, productive and social sustainability. This is said to be possible supporting traditional agriculture with new technologies like Geographic Information System (GIS), Global Navigation Satellites Systems (GNSS), digital photogrammetry and remote sensing. PA can therefore support farmers to maximize the cost-benefit ratio in yield production (Abdullahi et al., 2015; Lambert and Lowenberg-De Boer, 2000; Yousefi and Razdari, 2015). Prescription maps (PMs) are widely used in PA to map crop intra-field anomalies to better address fertilisation (Casa et al., 2011; Peerlinck et al., 2018; Radočaj et al., 2022), irrigation (Evett et al., 2020) and phytosanitary treatments (Hedley, 2015; Yang, 2020). The aim is minimizing negative externalities (i.e. water, air and soil pollution) and maximising yield (Sishodia et al., 2020). As far as remote sensing is concerned, multispectral information from aerial or space platforms can effectively support PMs generation (Chen et al., 2022; Lamb and Brown, 2001), depending on a proper choice of the adopted sensor in terms of spatial, spectral, radiometric and temporal resolution (Boccardo et al., 2003; Mondino et al., 2012). Besides those mentioned above, an additional element involved in the constitution of PM is the solar radiation reflected by the plants, which is strictly related to the chemical and morphological characteristics of the plant itself (Xue and Su, 2017). Therefore, plant type, water content, and canopy characteristics affect the light reflected (visible, ultraviolet, near and mid infrared portion) in a different way in each spectral band. Different sections of the electromagnetic spectrum, were commonly used to develop vegetation indices (VI) that provide useful information on plant structure and conditions (Samuele Petris et al., 2024; Xue and Su, 2017). VIs are mathematical expressions which combine the reflectance measured by the sensors in many spectral bands in order to generate a value, that summarises vegetation related information such as development, biomass and chlorophyll content (McKinnon and Hoff, 2017). It is well known in the literature that mapping VIs can support the analysis of crops spatio-temporal variability, which is key for PA applications. However, costs associated to aerial and RPAS (Remotely Piloted Aircraft Systems)-based acquisitions are known to be difficult to be estimated since strongly

* Corresponding author.
E-mail address: filippo.sarvia@unito.it (F. Sarvia).

https://doi.org/10.1016/j.ejrs.2024.06.003
Received 8 August 2022; Received in revised form 28 June 2023; Accepted 4 June 2024

dependent on the required data processing level and size of the imaged area (Borgogno Mondino and Gajetti, 2017; De Petris et al., 2020; Perz and Wronowski, 2019; Sarvia et al., 2021b). Fortunately, in addition to the spectral component, they can provide a very high spatial resolution typically ranging from 0.5 m to 1 cm and make possible 3D measures thanks to their stereoscopic capabilities (Ehlert et al., 2008; Hoffmeister et al., 2010). This peculiarity can be proficiently exploited to integrate spectral information. This can be generally achieved assuming digital surface models (or directly point clouds) as additional discriminants effective for deriving information about canopy and biomass of surveyed crops. In literature is well know that the canopy height model (CHM), representing the upper boundary of a cultivated field, can be useful for several PA applications (Hämmerle and Höfle, 2014). For example, by normalizing a CHM with a digital terrain model (DTM) representing the elevation of the bare soil, the crop height distribution can be derived and used in order to derive grain yield estimations (Lumme et al., 2008), leaf area index distribution (Dammer et al., 2008), assess crop fertilization status (Eitel et al., 2014; Viljanen et al., 2018) and generate crop biomass model (Tilly et al., 2014).

As far as multispectral features from RPAS sensors are concerned they certainly represent a potential breakthrough in PA. As we mentioned above, several spectral VI can be, in fact, generated for providing valuable vegetation-related information. Two of the mostly used VIs in PA are the Normalized Difference Vegetation Index (NDVI) and the Normalized Difference Red Edge Index (NDRE) (Rouse et al., 1974). They are known to be effective for monitoring of vegetation physiology (S. De Petris et al., 2024; Farbo et al., 2024; Li et al., 2019; Seo et al., 2019; Suwanlee et al., 2024, 2023), estimation of crop production (Huang et al., 2014; van Klompenburg et al., 2020; Wang et al., 2005), ecosystems characterization (Sarvia et al., 2021a), monitoring of crop nitrogen (N) content (Boiarskii and Hasegawa, 2019; Li et al., 2018; Song et al., 2020) and support the crop damage estimation within the insurance policies context (Borgogno-Mondino et al., 2019; F et al., 2020). An extensive list of multispectral imaging sensors can be easily found on market the most of them acquiring bands in the VNIR (400–1000 nm) spectral range. MAIA S2 (MS2) is one of the most performing ones in terms of spectral resolution. MS2 acquires 9 bands in the range 390–950 nm using 9 separated optical systems equipped with filters (Marinello, 2017) that are aligned to the ones of the Sentinel 2 MSI sensor (Ryan et al., 2018). Moreover, according to Segarra et al., (Segarra et al., 2020) MS2 and S2 data can be integrated for agricultural field analysis in a precision agriculture context.

Within this framework, in this work a corn field was analysed with the MAIAS2 (MS2) sensor equipped on a quadcopter RPAS. The field was previously sub-divided into three sections and a different nitrogen fertilisation dose was applied. Starting from MS2 multispectral image block bundle adjustment the NDVI, NDRE and CHM maps were used to assess the effects of fertilization treatments. For each map, an unsupervised classification was performed to generate a zoned maps. Since analysed subfields are affected by similar environmental conditions (i.e. soil, rainfall, temperature) but a different fertilisation doses was applied, the clusters obtained are expected to reflect the fertilization gradient. The consistency between the cluster maps (hereafter called CM) and fertilization treatments was finally tested.

2. Materials and methods

2.1. Study area and experimental plots

The study area (AOI) is in Carignano (Piemonte region – Italy) and sizes about 5 ha. AOI is characterized by a typical temperate climate with continental character. Furthermore, since the area is placed within the North-Western Alps, there is generally a gradual decrease in temperature with increasing altitude. Thermal inversion phenomena, caused by cold air, can often affect the area, especially in the valleys. Average annual temperature and precipitation are 11.9 °C and 1050 mm, respectively. The Piemonte region is highly devoted to agriculture and in particular in cereal production (Boori et al., 2019; Farbo et al., 2022; Ghilardi et al., 2022).

AOI corresponds to a corn field and an experimental test involving different nitrogen application during the development of the crop was carried out in 2021. Specifically, AOI has been divided into three plots (hereafter called A, B and C) that were fertilized with different doses of N-based mineral fertilizers: 0 kg • ha^{-1}N, 120 kg • ha^{-1}N and 240 kg • ha^{-1}N, respectively (Fig. 1). AOI was selected as representative of local agricultural corn management, being corn the most important crop in the area (Sarvia et al., 2022).

2.2. Aerial survey

An aerial survey was performed on 14th June 2021 using a quadcopter (DJI Matrice 300 RTK) equipped with MS2 sensor. At the same time, the phenological stage of corn can be identified as the stem elongation (BBCH scale 39). MS2 technical features are the following: focal length = 7.5 mm, physical pixel size = 3.75 μm, sensor size = 1280 × 960 mm. Forward and side overlap were set equal to 95 % and 90 % respectively and the aerial survey was performed @ 80 m AGL (above the ground level). The free software *Mission Planner v1.3.58* was used to plan the flight and set up the autopilot for the flight. Flight time resulted to be 15 min. Imaged area was about 10.30 ha corresponding to 1600 frames (raw format).

2.3. Ground surveys

To generate good photogrammetric point clouds (PPCs), an accurate image bundle adjustment is required (Triggs et al., 2000). This requires an adequate number of ground control points (GCPs), accurately surveyed and appropriately distributed in the area. For this reason, five GCPs were surveyed during the flight by GNSS (Fig. 2) operated in VRS-NRTK (Virtual Reference Station – Network Real Time Kinematic) mode supported by the Interregional Piemonte-Lombardia SPIN-GNSS service (https://www.spingnss.it/spiderweb/frmIndex.aspx). A GNSS receiver *Leica GX1200 system* was used for this task. The average 3D-positional accuracy was 35 mm and the final reference frame was WGS84/UTM 32 N. Moreover, to locally model with adequate accuracy the local ground level, 28 additional points, namely Terrain Points (TP), were surveyed and used to compute a digital terrain model needed for CHM generation. This was achieved spatially interpolating TPs by Delaunay triangulation in SAGA GIS 7.9 (Olaya and Conrad, 2009) obtaining a gridded digital terrain model (DTM) having a grid size of 0.1 m. Also in this case the reference frame was WGS84/UTM 32 N.

2.4. Data processing

The main conceptual steps of the proposed methodology are reported in Fig. 3. Involved steps are deeply explained in the following sections.

MS2 raw images were pre-processed by MultiCam Stitcher Pro v 1.4-Beta 2 (MCS). Images were geometrically corrected to remove/minimize distortions related to sensor lens system and design using the available automatic procedure in MCS. Nominal calibration parameters, different for each band, are recorded within MCS and automatically applied during processing (Nocerino et al., 2017). A co-registration step aiming at aligning bands was successively achieved and a multi-layer image, stacking 9 co-registered and undistorted bands was generated. During the process, radiance to reflectance conversion was operated using data from the MS2-coupled incident light sensor (ILS). Image block bundle adjustment was operated by *Agisoft Metashape v 1.7.4* (APS) using the above mentioned 5 GCPs. Camera auto-calibration was activated, fixing the focal length at its nominal value and estimating cx, cy, k1, k2, k3, k4 ("Agisoft PhotoScan User Manual – Professional Edition, Version 1.4," n.d.). A Leave One Out approach (Brovelli et al., 2008) was used to test 3D accuracy of image block orientation and vertical and horizontal

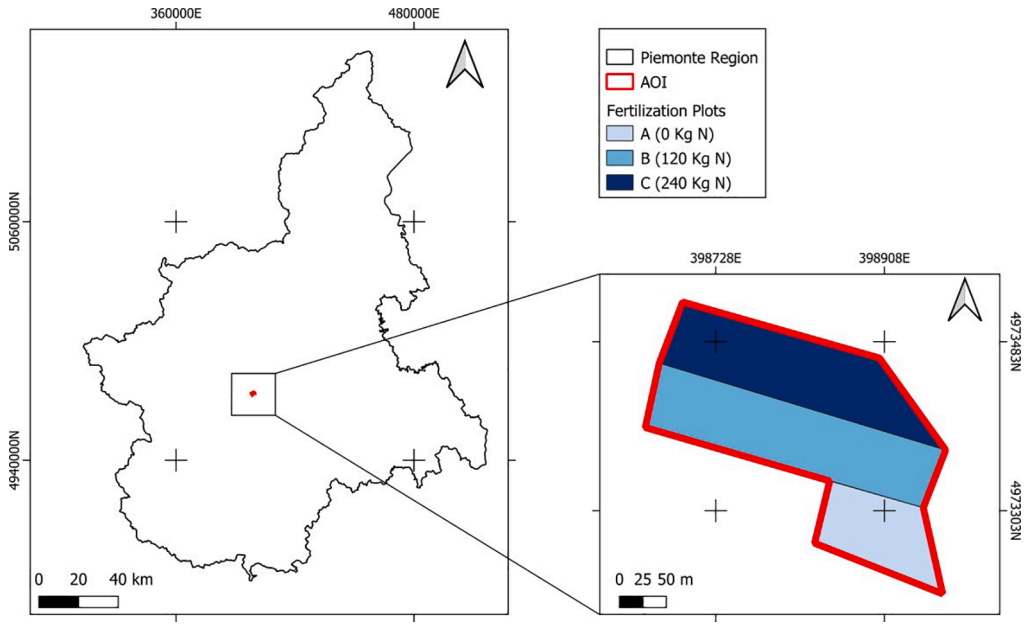

Fig. 1. Area of Interest (AOI) within Piemonte Region (N-W Italy) is represented by a red polygon. AOI was subdivided into three plots (A, B and C) which were treated with three levels of fertilization at the stem elongation stage (0, 120, 240 Kg N respectively). (Reference system WGS84 / UTM 32 N, EPSG: 32632).

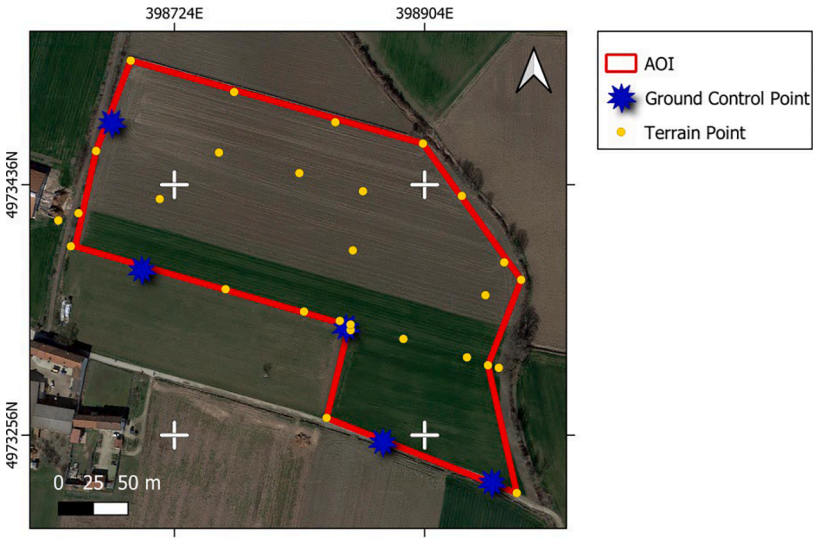

Fig. 2. Terrain Points and Ground Control Points acquired within the AOI. (Reference System WGS84/UTM 32 N, EPSG: 32632).

RMSE computed. A photogrammetric point cloud (PPC) sizing 17,013,157 points was generated and filtered to remove outliers. A raster Digital Surface Model (DSM) was then computed by regularization setting a GSD of 0.1 m. Finally, the correspondent MO was generated with a GSD of 0.05 m. The default images blending mode was used, admitting that native radiometry of images would have been distorted. Nevertheless, since the main task was zoning, authors preferred to guarantee a better spatial continuity of images that only a blending mode can guarantee. MO was projected into the WGS84 UTM 32 N reference frame. CHM, mapping the local crop height above the ground level, was computed by grid differencing between local DSM (from RPAS) and DTM (from GNSS survey). NDVI and NDRE (Bannari et al., 1995) maps were computed from the calibrated bands of MO by raster calculation. Given the high geometric resolution of MO and CHM, plants inter-row (equal to 0.75 m) was also detected thus introducing noise in a wall-to-wall mapping of crop properties. To reduce this limiting factor while zoning, a vector graticule sizing 1 m x 1 m was generated and zonal statistics computed with reference to the above mentioned NDVI, NDRE and CHM raster maps. Specifically, the local mean value was computed for NDVI and NDRE, while the local 95th percentile was computed from CHM. This was intended to transfer to the 1 m x 1 m graticule cell the information about the top of the canopy, thus excluding plants inter-rows related heights. Downsampled NDVI, NDRE and CHM were used to derive a zonation of the field possibly corresponding to the three doses of N. Resulting maps can be somehow intended as the basis for deriving prescription maps – PMs (Bates et al., 2018) useful for a variable rate-based field management. Zonation was achieved by unsupervised classification of NDVI, NDRE and CHM (singularly considered). The K-means clustering was applied looking for 3 clusters (expected to reflect crop high, medium and low vigour conditions). Since in a cluster analysis class meaning is not a-priori known, to recover it, the mean and standard deviation values (NDVI, NDRE and CHM) were *a-posteriori* computed for each cluster and interpreted with the following interpretation keys: (i) high vigour class is the one

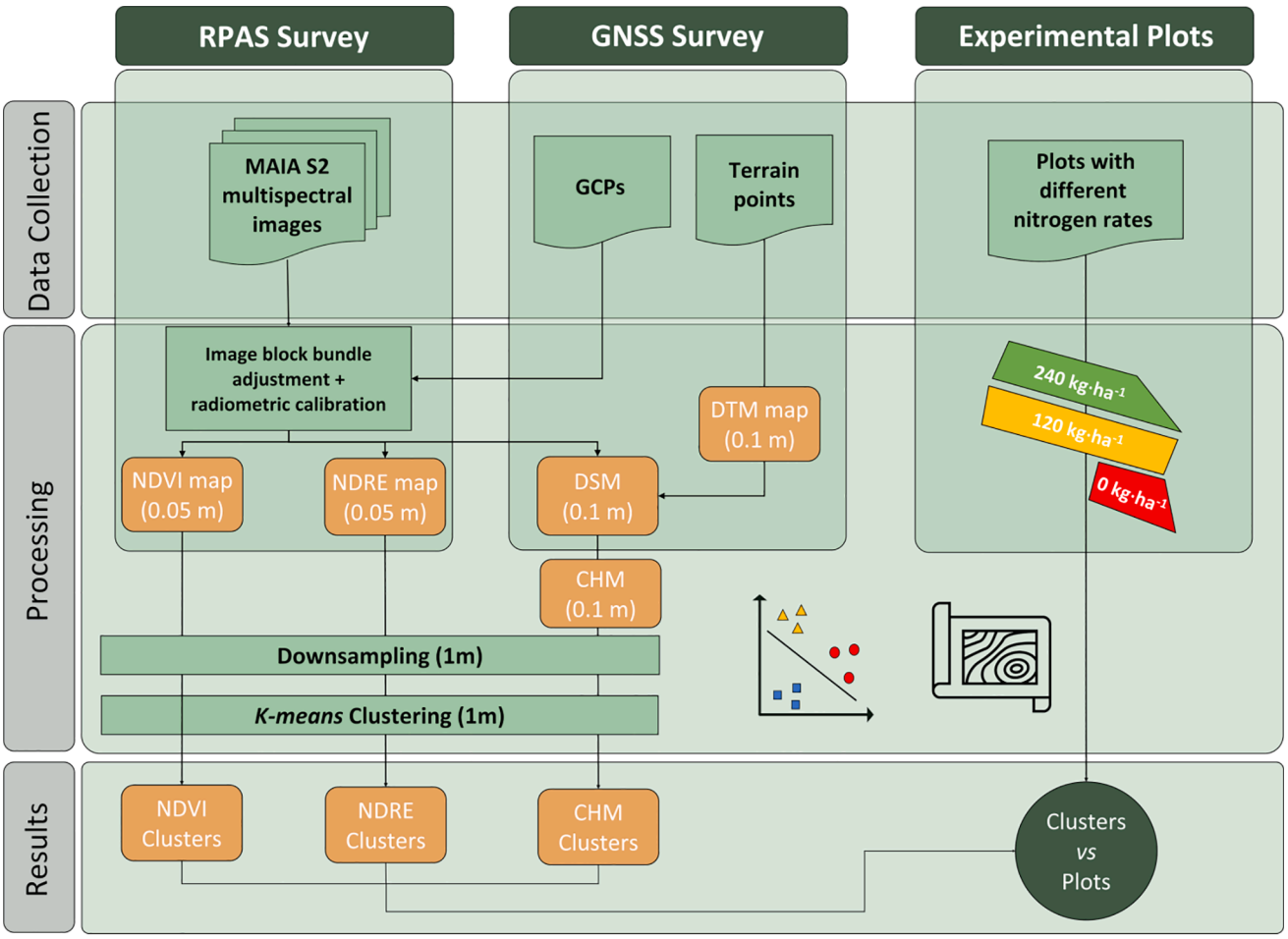

Fig. 3. Main conceptual steps of the proposed methodology.

showing the highest mean NDVI, NDRE and CHM values; (ii) low vigour class is the one showing the lowest NDVI, NDRE and CHM values; (iii) medium vigour class is the intermediate one. Differences affecting corn field development can be reasonably ascribed to the N fertilization since environmental conditions can be assumed similar over AOI sub-plots. For this reason: field A (N = 0 kg • ha^{-1}), field B (N = 120 kg • ha^{-1}) and field C (N = 240 kg • ha^{-1}) were expected to correspond to the low, medium and high vigour class, respectively. It is worth to remind that a corn field is an open and unlimited context where nutrient exchange at soil level and among-plants competition during the growth phase can occur (Cahill Jr, 1999). To test truthfulness of their hypothesis, authors proceeded by polygon intersection locally comparing CMs classes with A, B and C plots and looking for the highest occurrences.

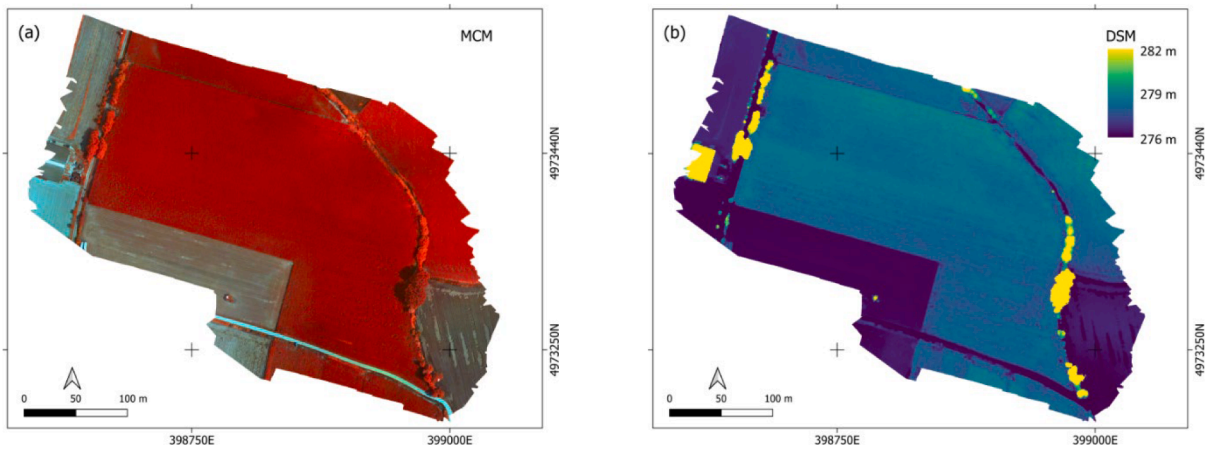

Fig. 4. (a) False colour composite from MO (R: NIR band, G: Red band, B: Green band). (b) Digital surface model. (Reference System WGS84/UTM 32 N, EPSG: 32632).

3. Results and discussions

3.1. Data processing

Accuracy of bundle adjustment was found to be 0.02 m (horizontal) and 0.03 m (vertical). These accuracy values well fits PA requirements (Rokhmana, 2015) especially when the geometric 3D content of images is expected to be exploited to derive useful information about crops. The obtained dense cloud (PPC) sizing 17,013,157 points. It was then regularized with a GSD = 0.1 m to generate the correspondent DSM (Fig. 4b). Finally, DSM was used to generate MO having a GSD = 0.1 m, as well. This was used to generate the NDVI and NDRE maps.

With reference to the DTM from ground surveyed TPs it was used to derive crop CHM (Fig. 5). The mean CHM value in AOI was found to be 2.5 m in agreement with the expected corn height reached in the heading phenological phase (June). Similar results were also found by Tirado et al. in which the height of 12 different maize hybrids was measured and estimated with a UAV (Tirado et al., 2020). Their research results highlighted an average corn height of 2.5 m, confirming corn vigour observed in this work.

Zonal statistics were applied with reference to the above mentioned 1 m x 1 m cell graticule to downsample NDVI, NDRE and CHM maps, thus minimizing local effects (on both radiometry and geometry) from plants inter-row. K-means clustering (3 clusters) was singularly applied for the obtained downsampled NDVI, NDRE and CHM maps (Fig. 5). To recover cluster meaning, an intersection was achieved between clusters and management zones (A,B,C). Meaning correspondence was obtained looking at occurrences of combinations. Corn development and relative biomass were expected to be high, medium and low for the respective A, B and C areas. Occurrences (%), mean and standard deviation values of class combinations are reported in Table 1. CM from NDVI shows that A, B and C were characterised by a mean NDVI value of 0.88, 0.94 and 0.97, respectively (Tab.1). CM from NDRE, differently, shows that A, B and C were characterised by having an average NDRE value of 0.22, 0.25 and 0.27 respectively. CM from CHM shows that A, B and C were characterised by an average canopy height value of 2.21 m, 2.58 m and 2.96 m respectively. Based on these results, CM vigour levels (managed plots) can be associated to the corresponding clusters. Specifically, vigour levels appear to be high, medium and low respectively for C, B and A in all CMs. Finally, the effects of fertilisation detected by CMs were evaluated and the relative statistical distribution reported in Fig. 6.

According to Fig. 6a, CM from NDVI appears to be mainly dominated by the high vigour class. Specifically, plot A, B and C are characterized by having predominance of high vigour class (53 %, 70 % and 92 % respectively). Concerning CM form NDRE, plot A, B and C are, respectively, characterized by mid-low, medium and high vigour classes

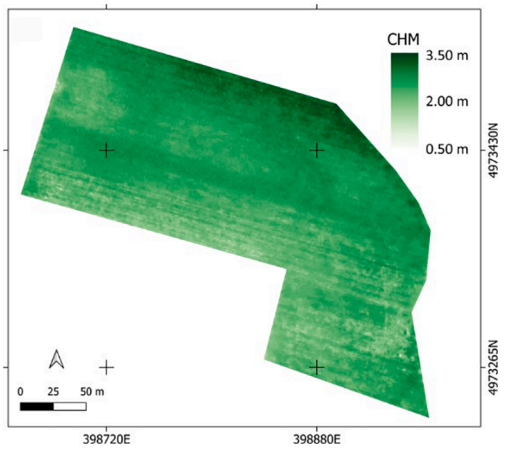

Fig. 5. Canopy Height Model of the imaged corn field. (Reference System WGS84/UTM 32 N, EPSG: 32632).

Table 1
Number of pixels and relative %, mean and standard deviation values of clusters from NDVI, NDRE and CHM maps.

Index	Number of Pixels	Pixels (%)	Mean	Standard deviation	Field treatment
NDVI	35,184	75.54 %	0.97	0.01	C
	8632	18.53 %	0.94	0.01	B
	2763	5.93 %	0.88	0.03	A
NDRE	18,128	38.92 %	0.27	0.01	C
	19,694	42.28 %	0.25	0.01	B
	8757	18.80 %	0.22	0.01	A
CHM	8218	17.68 %	2.96	0.16	C
	22,650	48.72 %	2.58	0.10	B
	15,625	33.61 %	2.21	0.14	A

(46–40 %, 46 % and 60 %). Finally, CM from CHM shows that plot A, B and C are, respectively, characterized by low, medium and medium–high vigour classes (61 %, 51 % and 50–41 %).

Based on this results, one can deduce that CM from NDVI appears to poorly detect N-related differences rising some doubts about NDVI applications in CM generation during corn late phenological phases. Conversely, NDRE- and CHM-derived CMs reasonably reflect the different N fertilizations rates. It is worth to remind that whatever cluster map would never perfectly fit the N-fertilization plots, since transition zones between treatments (Chekli et al., 2017; Kim et al., 2019) are always present as a natural consequence of treatments dynamics in the environment.

Findings from this work are supported by recent literature (Feng et al., 2016) where (i) NDRE is shown to be correlated with different leaf N concentration; (ii) N content of vegetation is better detected by NDRE rather than NDVI (Boiarskii and Hasegawa, 2019). Specifically, Barker and Sawyer assess corn N fertilization by establishing canopy indices on corn fields from 2006 to 2008 (62 site-years) located in Iowa State University Research and Demonstration Farms (Barker and Sawyer, 2010). Their results highlight that several indices related to the canopy biomass (such as the CHM) can be used to monitor and generate N rate algorithm for applying N fertilizer in-season. Yu, Wand and Leblon studied the relationship between the spatial variation of canopy nitrogen weight and factors such as plant height, topographic metrics, soil chemical properties, and soil moisture conditions within a corn field in Southwestern Ontario using multispectral UAV-based imagery (Yu et al., 2021). Despite they used several variables (geometric, topographic and spectral), the most important one turned out to be the height of the corn. Therefore, according to findings of this work and the above-mentioned literature, what actually is relevant is that the geometric information related to crop CHM can be proficiently used as further, or alternative, detecting tool suggesting that, for this type of applications, low-cost RGB sensors (Grenzdörffer, 2014), properly managed within a digital photogrammetric workflow, can provide similar, or complementary, information about crops in the PA framework.

4. Conclusions

To explore the potentiality of MS2 from drones for generating useful information in agriculture, a pilot experience was achieved focusing on a corn field managed with three different N fertilisation doses. MS2 were geometrically and spectrally pre-processed and the related multispectral orthomosaic and digital surface model, derived. The former was used to compute the correspondent NDVI and NDRE maps. The latter was differently used to derive a corn canopy height model. An unsupervised classification approach @3 clusters was then applied to NDVI, NDRE and CHM maps to zone the field. Zones from clustering were therefore compared with field sections at different N doses to test capacity of the above mentioned spectral and geometric discriminants to map differences. Results suggest that CM from NDVI appears to poorly detect N-related differences. Contrarily, CMs from NDRE and CHM reasonably

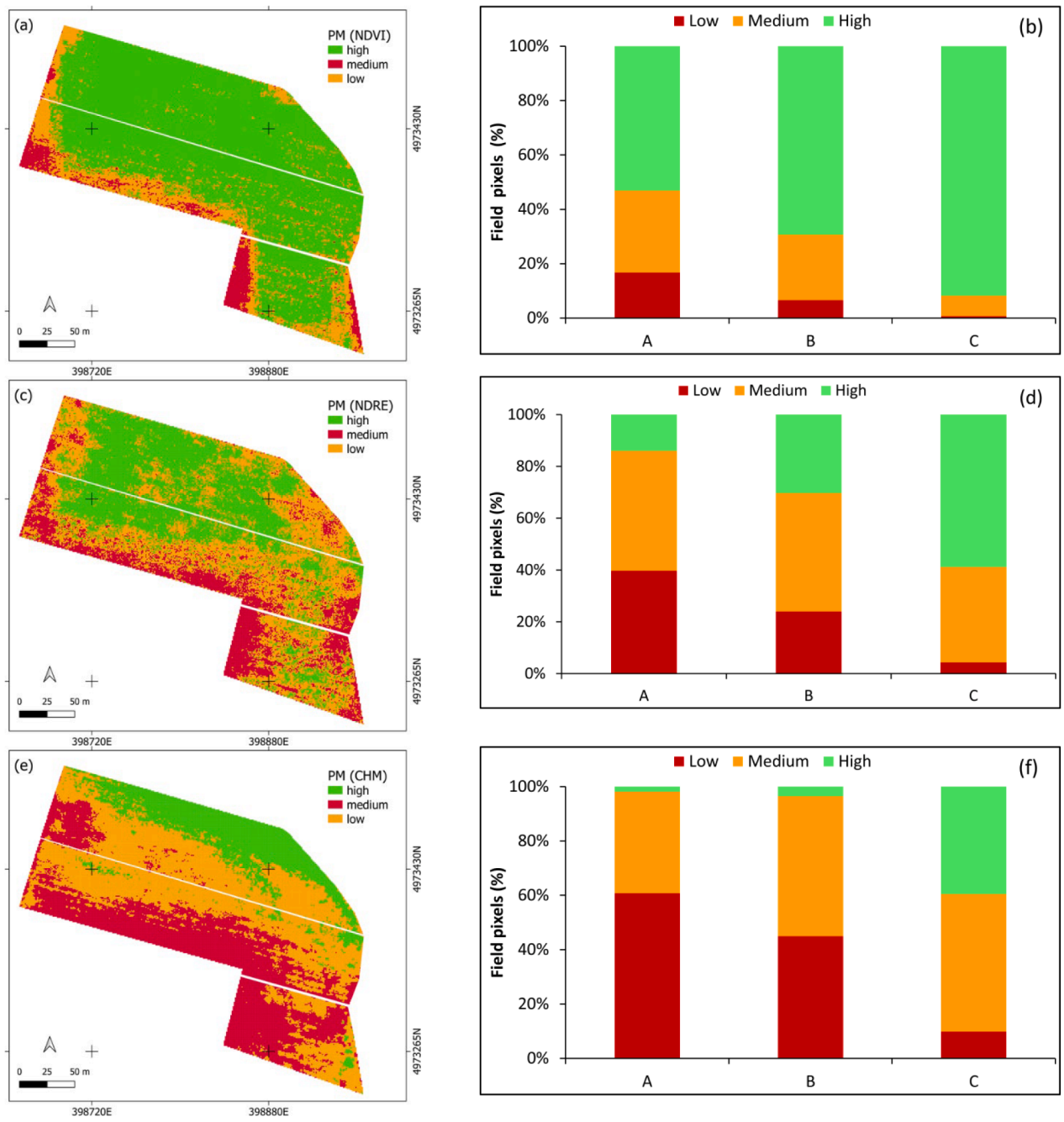

Fig. 6. (a) Prescription map generated from the NDVI map. (b) Statistical distribution of vigour classes derived by CM (NDVI) for the different fertilisation test applied in the corn field. (c) Prescription map generated starting from the NDRE map. (d) Statistical distribution of vigour classes derived by CM (NDRE) for the different fertilisation test applied in the corn field. (f) Statistical distribution of vigour classes derived by CM (CHM) for the different fertilisation test applied in the corn field. (Reference System WGS84/UTM 32 N, EPSG: 32632).

reflect the different N fertilization doses. Specifically, CHM proved to be able to detect crop height and, consequently, biomass differences that are known to be induced by different rates of fertilization. What actually is relevant is that the geometric information related to crop CHM can be proficiently used as further, or alternative, detecting tool suggesting that, for this type of applications, low-cost RGB sensors can provide similar, or complementary, information about crops in the PA framework.

Funding

This research was funded by TELECER – Applicazione del telerilevamento per il miglioramento produttivo e qualitativo dei cereali per le filiere avanzate – Bando FEASR – Programma di Sviluppo Rurale 2014–2020 (PSR) Regione Piemonte.

Declaration of Competing Interest

The authors declare that they have no known competing financial interests or personal relationships that could have appeared to influence the work reported in this paper.

References

Abdullahi, H.S., Mahieddine, F., Sheriff, R.E., 2015. Technology impact on agricultural productivity: A review of precision agriculture using unmanned aerial vehicles, in: Wireless and Satellite Systems: 7th International Conference, WiSATS 2015, Bradford, UK, July 6-7, 2015. Revised Selected Papers 7. Springer, pp. 388–400.

Bannari, A., Morin, D., Bonn, F., Huete, A., 1995. A review of vegetation indices. Remote Sens. Rev. 13, 95–120.

Barker, D.W., Sawyer, J.E., 2010. Using active canopy sensors to quantify corn nitrogen stress and nitrogen application rate. Agron. J. 102, 964–971.

Bates, T., Dresser, J., Eckstrom, R., Badr, G., Betts, T., Taylor, J., 2018. Variable-rate mechanical crop adjustment for crop load balance in "Concord" vineyards. Presented at the 2018 IoT Vertical and Topical Summit on Agriculture - Tuscany. IOT Tuscany 2018, 1–4. https://doi.org/10.1109/IOT-TUSCANY.2018.8373046.

Boccardo, P., Mondino, E.B., Tonolo, F.G., 2003. High resolution satellite images position accuracy tests. In: IGARSS 2003. 2003 IEEE International Geoscience and Remote Sensing Symposium. Proceedings (IEEE Cat, No. 03CH37477). IEEE, pp. 2320–2322.

Boiarskii, B., Hasegawa, H., 2019. Comparison of NDVI and NDRE indices to detect differences in vegetation and chlorophyll content. J. Mech. Continua Mathe. Sci. 4, 20–29.

Boori, M.S., Choudhary, K., Paringer, R., Sharma, A.K., Kupriyanov, A., Corgne, S., 2019. Monitoring crop phenology using NDVI time series from sentinel 2 satellite data, in: 2019 5th International Conference on Frontiers of Signal Processing (ICFSP). IEEE, pp. 62–66.

Borgogno Mondino, E., Gajetti, M., 2017. Preliminary considerations about costs and potential market of remote sensing from UAV in the Italian viticulture context. European J. Remote Sensing 50, 310–319.

Borgogno-Mondino, E., Sarvia, F., Gomarasca, M.A., 2019. Supporting insurance strategies in agriculture by remote sensing: a possible approach at regional level. In: International Conference on Computational Science and Its Applications. Springer, pp. 186–199.

Brovelli, M.A., Crespi, M., Fratarcangeli, F., Giannone, F., Realini, E., 2008. Accuracy assessment of high resolution satellite imagery orientation by leave-one-out method. ISPRS J. Photogramm. Remote Sens. 63, 427–440.

Cahill Jr, J.F., 1999. Fertilization effects on interactions between above-and belowground competition in an old field. Ecology 80, 466–480.

Casa, R., Cavalieri, A., Cascio, B.L., 2011. Nitrogen fertilisation management in precision agriculture: a preliminary application example on maize. Ital. J. Agron. 6, e5–e.

Chekli, L., Kim, Y., Phuntsho, S., Li, S., Ghaffour, N., Leiknes, T., Shon, H.K., 2017. Evaluation of fertilizer-drawn forward osmosis for sustainable agriculture and water reuse in arid regions. J. Environ. Manage. 187, 137–145.

Chen, F., Zhang, Y., Zhang, J., Liu, L., Wu, K., 2022. Rice false smut detection and prescription map generation in a complex planting environment, with mixed methods, based on near earth remote sensing. Remote Sens. (Basel) 14, 945.

Dammer, K.-H., Wollny, J., Giebel, A., 2008. Estimation of the Leaf Area Index in cereal crops for variable rate fungicide spraying. Eur. J. Agron. 28, 351–360.

De Petris, S., Sarvia, F., Borgogno-Mondino, E., 2020. RPAS-based photogrammetry to support tree stability assessment: longing for precision arboriculture. Urban For. Urban Green. 55, 126862 https://doi.org/10.1016/j.ufug.2020.126862.

De Petris, S., Sarvia, F., Parizia, F., Ghilardi, F., Farbo, A., Borgogno-Mondino, E., 2024. Assessing mixed-pixels effects in vineyard mapping from Satellite: a proposal for an operational solution. Comput. Electron. Agric. 222, 109092 https://doi.org/10.1016/j.compag.2024.109092.

De Petris, Samuele, Sarvia, F., Borgogno-Mondino, E., 2024. About polygon area uncertainty in GIS and its implications on agro-forestry estimates. Eco. Inform. 81, 102617.

Ehlert, D., Horn, H.-J., Adamek, R., 2008. Measuring crop biomass density by laser triangulation. Comput. Electron. Agric. 61, 117–125.

Eitel, J.U., Magney, T.S., Vierling, L.A., Brown, T.T., Huggins, D.R., 2014. LiDAR based biomass and crop nitrogen estimates for rapid, non-destructive assessment of wheat nitrogen status. Field Crop Res 159, 21–32.

Evett, S.R., O'Shaughnessy, S.A., Andrade, M.A., Kustas, W.P., Anderson, M.C., Schomberg, H.H., Thompson, A., 2020. Precision agriculture and irrigation: Current US perspectives. Trans. ASABE 63, 57–67.

F, S., S, D.P., E, B.-M., 2020. Multi-scale remote sensing to support insurance policies in agriculture: from mid-term to instantaneous deductions. null 57, 770–784. https://doi.org/10.1080/15481603.2020.1798600.

Farbo, A., Sarvia, F., De Petris, S., Borgogno-Mondino, E., 2022. Preliminary Concerns About Agronomic Interpretation of Ndvi Time Series from Sentinel-2 Data: Phenology and Thermal Efficiency of Winter Wheat in Piemonte (nw Italy). In: The International Archives of Photogrammetry, Remote Sensing and Spatial Information Sciences. Copernicus GmbH, Gottingen, Germany, pp. 863–870. https://doi.org/10.5194/isprs-archives-XLIII-B3-2022-863-2022.

Farbo, A., Sarvia, F., De Petris, S., Basile, V., Borgogno-Mondino, E., 2024. Forecasting corn NDVI through AI-based approaches using sentinel 2 image time series. ISPRS J. Photogramm. Remote Sens. 211, 244–261. https://doi.org/10.1016/j.isprsjprs.2024.04.011.

Feng, W., Zhang, H.-Y., Zhang, Y.-S., Qi, S.-L., Heng, Y.-R., Guo, B.-B., Ma, D.-Y., Guo, T.-C., 2016. Remote detection of canopy leaf nitrogen concentration in winter wheat by using water resistance vegetation indices from in-situ hyperspectral data. Field Crop Res 198, 238–246.

Ghilardi, F., Petris, S.D., Farbo, A., Sarvia, F., Borgogno-Mondino, E., 2022. Exploring Stability of Crops in Agricultural Landscape Through GIS Tools and Open Data. In: Gervasi, O., Murgante, B., Misra, S., Rocha, A.M.A.C., Garau, C. (Eds.), Computational Science and Its Applications – ICCSA 2022 Workshops. Springer International Publishing, Cham, pp. 327–339. https://doi.org/10.1007/978-3-031-10545-6_23.

Grenzdörffer, G.J., 2014. Crop height determination with UAS point clouds. The International Archives of Photogrammetry, Remote Sensing and Spatial Information Sciences 40, 135.

Hämmerle, M., Höfle, B., 2014. Effects of reduced terrestrial LiDAR point density on high-resolution grain crop surface models in precision agriculture. Sensors 14, 24212–24230.

Hedley, C., 2015. The role of precision agriculture for improved nutrient management on farms. J. Sci. Food Agric. 95, 12–19.

Hoffmeister, D., Bolten, A., Curdt, C., Waldhoff, G., Bareth, G., 2010. High-resolution Crop Surface Models (CSM) and Crop Volume Models (CVM) on field level by terrestrial laser scanning, in: Sixth International Symposium on Digital Earth: Models, Algorithms, and Virtual Reality. SPIE, pp. 90–95.

Huang, J., Wang, H., Dai, Q., Han, D., 2014. Analysis of NDVI data for crop identification and yield estimation. IEEE J. Sel. Top. Appl. Earth Obs. Remote Sens. 7, 4374–4384.

Kim, Y., Li, S., Phuntsho, S., Xie, M., Shon, H.K., Ghaffour, N., 2019. Understanding the organic micropollutants transport mechanisms in the fertilizer-drawn forward osmosis process. J. Environ. Manage. 248, 109240.

Lamb, D.W., Brown, R.B., 2001. Pa—precision agriculture: Remote-sensing and mapping of weeds in crops. J. Agric. Eng. Res. 78, 117–125.

Lambert, D., Lowenberg-De Boer, J., 2000. Precision agriculture profitability review. Purdue Univ, West Lafayette, IN.

Li, S., Ding, X., Kuang, Q., Ata-UI-Karim, S.T., Cheng, T., Liu, X., Tian, Y., Zhu, Y., Cao, W., Cao, Q., 2018. Potential of UAV-based active sensing for monitoring rice leaf nitrogen status. Front. Plant Sci. 9, 1834.

Li, C., Li, H., Li, J., Lei, Y., Li, C., Manevski, K., Shen, Y., 2019. Using NDVI percentiles to monitor real-time crop growth. Comput. Electron. Agric. 162, 357–363.

Lumme, J., Karjalainen, M., Kaartinen, H., Kukko, A., Hyyppä, J., Hyyppä, H., Jaakkola, A., Kleemola, J., 2008. Terrestrial laser scanning of agricultural crops. Int. Arch. Photogramm. Remote Sens. Spat. Inf. Sci 37, 563–566.

Marinello, F., 2017. Last generation instrument for agriculture multispectral data collection. Agric. Eng. Int. CIGR J. 19, 87–93.

McKinnon, T., Hoff, P., 2017. Comparing RGB-based vegetation indices with NDVI for drone based agricultural sensing. Agribotix. Com 21, 1–8.

Mondino, E.B., Perotti, L., Piras, M., 2012. High resolution satellite images for archeological applications: the Karima case study (Nubia region, Sudan). European J. Remote Sensing 45, 243–259.

Nocerino, E., Dubbini, M., Menna, F., Remondino, F., Gattelli, M., Covi, D., 2017. Geometric calibration and radiometric correction of the maia multispectral camera. International Archives of the Photogrammetry, Remote Sensing & Spatial Information Sciences 42.

Olaya, V., Conrad, O., 2009. Geomorphometry in SAGA. Dev. Soil Sci. 33, 293–308.

Peerlinck, A., Sheppard, J., Maxwell, B., 2018. Using deep learning in yield and protein prediction of winter wheat based on fertilization prescriptions in precision agriculture. In: International Conference on Precision Agriculture (ICPA).

Perz, R., Wronowski, K., 2019. UAV application for precision agriculture. Aircr. Eng. Aerosp. Technol.

Radočaj, D., Jurišić, M., Gašparović, M., 2022. The role of remote sensing data and methods in a modern approach to fertilization in precision agriculture. Remote Sens. (Basel) 14, 778.

Rokhmana, C.A., 2015. The potential of UAV-based remote sensing for supporting precision agriculture in Indonesia. Procedia Environ. Sci. 24, 245–253.

Rouse, J.W., Haas, R.H., Schell, J.A., Deering, D.W., Harlan, J.C., 1974. Monitoring the vernal advancement and retrogradation (green wave effect) of natural vegetation. NASA/GSFC Type III Final Report, Greenbelt, Md, p. 371.

Ryan, C.G., Kirkham, R., Moorhead, G., Parry, D., Jensen, M., Faulks, A., Hogan, S., Dunn, P., Dodanwela, R., Fisher, L., et al., 2018. Maia Mapper: High definition XRF imaging in the lab. J. Instrum. 13, C03020.

Sarvia, F., De Petris, S., Borgogno-Mondino, E., 2021a. Exploring climate change effects on vegetation phenology by MOD13Q1 Data: the piemonte region case study in the period 2001–2019. Agronomy 11, 555. https://doi.org/10.3390/agronomy11030555.

Sarvia, F., Petris, S.D., Orusa, T., Borgogno-Mondino, E., 2021b. MAIA S2 Versus Sentinel 2: Spectral Issues and Their Effects in the Precision Farming Context. In: In: International Conference on Computational Science and Its Applications. Springer, pp. 63–77.

Sarvia, F., De Petris, S., Ghilardi, F., Xausa, E., Cantamessa, G., Borgogno-Mondino, E., 2022. The importance of agronomic knowledge for crop detection by sentinel-2 in the cap controls framework: a possible rule-based classification approach. Agronomy 12, 1228. https://doi.org/10.3390/agronomy12051228.

Segarra, J., Buchaillot, M.L., Araus, J.L., Kefauver, S.C., 2020. Remote sensing for precision agriculture: Sentinel-2 improved features and applications. Agronomy 10, 641.

Seo, B., Lee, J., Lee, K.-D., Hong, S., Kang, S., 2019. Improving remotely-sensed crop monitoring by NDVI-based crop phenology estimators for corn and soybeans in Iowa and Illinois, USA. Field Crop Res 238, 113–128.

Sishodia, R.P., Ray, R.L., Singh, S.K., 2020. Applications of remote sensing in precision agriculture: a review. Remote Sens. (Basel) 12, 3136.

Song, X., Xu, D.-Y., Huang, S.-M., Huang, C.-C., Zhang, S.-Q., Guo, D.-D., Zhang, K.-K., Yue, K., 2020. Nitrogen content inversion of wheat canopy leaf based on ground spectral reflectance data. Ying Yong Sheng tai xue bao=. J. Appl. Ecol. 31, 1636–1644.

Suwanlee, S.R., Keawsomsee, S., Pengjunsang, M., Homtong, N., Prakobya, A., Borgogno-Mondino, E., Sarvia, F., Som-ard, J., 2023. Monitoring agricultural land and land

cover change from 2001–2021 of the chi river basin, thailand using multi-temporal landsat data based on google earth engine. Remote Sens. (Basel) 15, 4339.
Suwanlee, S.R., Pinasu, D., Som-ard, J., Borgogno-Mondino, E., Sarvia, F., 2024. Estimating sugarcane aboveground biomass and carbon stock using the combined time series of sentinel data with machine learning algorithms. Remote Sens. (Basel) 16, 750.
Tilly, N., Hoffmeister, D., Cao, Q., Huang, S., Lenz-Wiedemann, V., Miao, Y., Bareth, G., 2014. Multitemporal crop surface models: accurate plant height measurement and biomass estimation with terrestrial laser scanning in paddy rice. J. Appl. Remote Sens. 8, 083671.
Tirado, S.B., Hirsch, C.N., Springer, N.M., 2020. UAV-based imaging platform for monitoring maize growth throughout development. Plant Direct 4, e00230.
Triggs, B., McLauchlan, P.F., Hartley, R.I., Fitzgibbon, A.W., 2000. Bundle adjustment—a modern synthesis, in: Vision Algorithms: Theory and Practice: International Workshop on Vision Algorithms Corfu, Greece, September 21–22, 1999 Proceedings. Springer, pp. 298–372.
van Klompenburg, T., Kassahun, A., Catal, C., 2020. Crop yield prediction using machine learning: a systematic literature review. Comput. Electron. Agric. 177, 105709.
Viljanen, N., Honkavaara, E., Näsi, R., Hakala, T., Niemeläinen, O., Kaivosoja, J., 2018. A novel machine learning method for estimating biomass of grass swards using a photogrammetric canopy height model, images and vegetation indices captured by a drone. Agriculture 8, 70.
Wang, J., Rich, P.M., Price, K.P., Kettle, W.D., 2005. Relations between NDVI, grassland production, and crop yield in the central Great Plains. Geocarto Int. 20, 5–11.
Xue, J., Su, B., 2017. Significant remote sensing vegetation indices: A review of developments and applications. Journal of sensors 2017.
Yang, C., 2020. Remote sensing and precision agriculture technologies for crop disease detection and management with a practical application example. Engineering 6, 528–532.
Yousefi, M.R., Razdari, A.M., 2015. Application of GIS and GPS in precision agriculture (a review). Int. J. Adv. Biol. Biomed. Res. 3, 7–9.
Yu, J., Wang, J., Leblon, B., 2021. Evaluation of soil properties, topographic metrics, plant height, and unmanned aerial vehicle multispectral imagery using machine learning methods to estimate canopy nitrogen weight in corn. Remote Sens. (Basel) 13, 3105.